Large Eddy Simulation of Pressure Distribution of Fluid Flow Over Ridges of Circular, Parabolic and Rectangular Shapes

A.J. TEMPLEMAN AND M.G. RASUL*
School of Engineering and Built Environment, Faculty of Sciences, Engineering and Health
Central Queensland University, Queensland 4702
AUSTRALIA
*E-mail of corresponding author: m.rasul@cqu.edu.au

Abstract: - This paper presents modeling and large eddy simulation of pressure coefficient distribution of the flow of air over ridges of circular, parabolic and rectangular shapes at different Reynolds numbers using computational fluid dynamics (CFD) code FLUENT. The simulated results are compared and discussed with the experimentally measured pressure distributions. The experiments were done in an open circuit blower type wind tunnel. This study found that the pressure coefficient distributions over the three ridges are not unique in character at zero angle of attack for same Reynolds number and its magnitude depends on the geometry of the ridges. The typical potential flow equations are not applicable to predict the distance of pressure dissipation in the downstream direction of the flow.

Key-Words: - CFD simulation, ridges, pressure coefficient distribution

1 Introduction

It is widely known that when fluid flows externally past an immersed body, the body experiences a resultant force due to the interaction between the body and the fluid surrounding it. The resultant force can be expressed as the theory of drag, the numerical theory of drag is weak and inadequate because of flow separation. The boundary layer theory can predict the separation point but cannot accurately estimate the pressure distribution in the separation region. The difference between the high pressure in the front stagnation region and the low pressure in the rear separated region causes a large drag contribution call pressure drag. With the advances in computational fluid dynamics (CFD) simulation software, modelling and simulation of this resultant force has become possible.

The purpose of this study is to simulate pressure distribution of fluid flow over ridges of circular, parabolic and rectangular shapes using CFD code FLUENT. There have been many numerical and experimental studies on the fluid flow over ridges. However, it should be noted that using CFD does not necessarily ensure accurate results [1, 2]. Therefore the results obtain from CFD simulation should be verified with measured data. This paper presents large eddy simulation of pressure distribution of fluid flow over ridges of circular, parabolic and rectangular shapes using CFD code FLUENT. The simulated results are then compared with measured data and discussed.

2 Simulation of Pressure Distribution Over Ridges

The basic method for creating CFD simulation is represented in six main stages, as illustrated in Fig.1. These stages can be divided into three processes; pre-processing, solving and post-processing.

2.1 Gambit details

Gambit is a geometric and meshing software package that has seen designed to provide the capabilities to build and mesh models for import into CFD software. To determine the pressure coefficient distribution for comparison, the three ridges has been modelled in a wind tunnel. The geometry of this wind tunnel used was 5.04 × 0.3 × 0.2 metres. The ridges are each located 4 metres from the entrance of the wind tunnel. The geometry for the circular, parabolic and rectangular ridges are shown in Figs. 2, 3 and 4 respectively. Once the three ridges geometry was created in Gambit the next stage was to mesh it and to determine whether the models are mesh dependent or independent. The initial mesh sizes used were; for circular 31,310; for parabolic 40,672 and for rectangular 90,272. The initial mesh for rectangular ridge is shown in Fig. 5. These mesh sizes (for all ridges) were later approximately doubled in Fluent, to produce more accurate results.

2.2 Governing Equations and Simulation Techniques

The governing equations of fluid flow represent mathematical statements of the following conservation laws of physics [4]:

- The mass of a fluid is conserved
- The rate of change of momentum equals the sum of the forces on a fluid particle (Newton's second law)
- The rate of change of energy is equal to the sum of the rate of heat addition to and the rate of work done on a fluid particle (first law of thermodynamics).

The Naiver-Stokes equations and the Continuity equation which describe the dynamics of fluid flow are derived from the basic principles described above.

The Continuity equation can be derived from the Divergence theorem developed by Carl Friedrich Gauss in 1813.

$$\frac{\partial \rho}{\partial t} + \vec{\nabla} \cdot \left(\rho \vec{V} \right) = 0$$

The fluid is considered to be incompressible, thus the mean density will not change, and as a result the dynamic viscosity and kinematic viscosity are also considered constant. The continuity equation noted above can be expressed in Cartesian coordinates as,

$$\frac{\partial \rho}{\partial t} + \frac{\partial(\rho u)}{\partial x} + \frac{\partial(\rho v)}{\partial y} + \frac{\partial(\rho w)}{\partial z} = 0$$

Since it has been assumed that the fluid is incompressible, density is not a function of time or space [5]. Therefore $\frac{\partial \rho}{\partial t} \cong 0$ and density can be taken outside the divergence operator.

Incompressible continuity equation can be written as,

$$\frac{\partial u}{\partial x} + \frac{\partial v}{\partial y} + \frac{\partial w}{\partial z} = 0$$

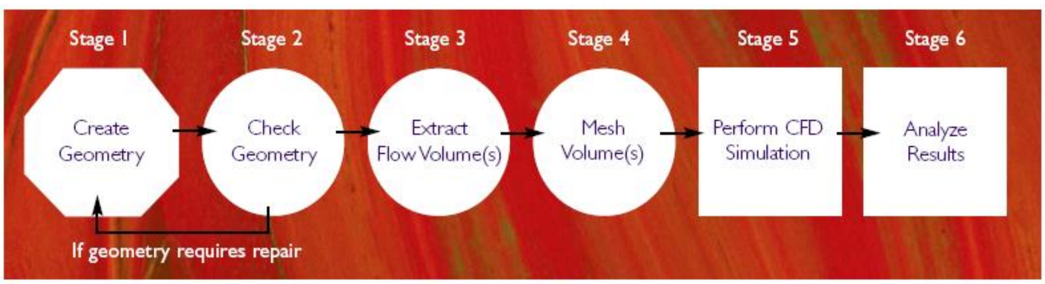

Fig. 1: Fluent CFD simulation process [3]

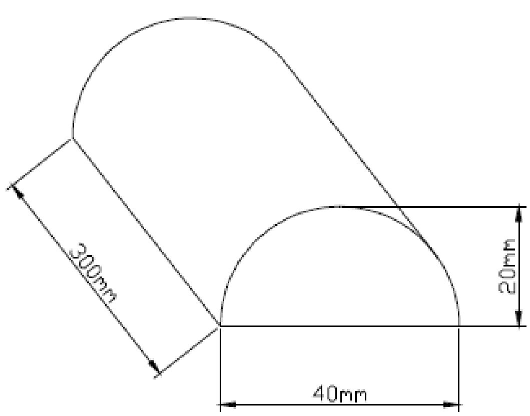

Fig. 2: Geometry of circular ridge

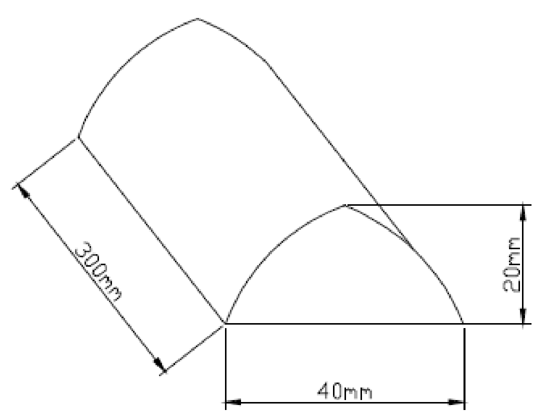

Fig. 3: Geometry of parabolic ridge

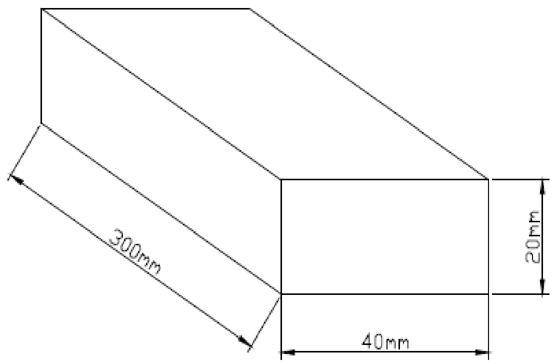

Fig. 4: Geometry of rectangular ridge

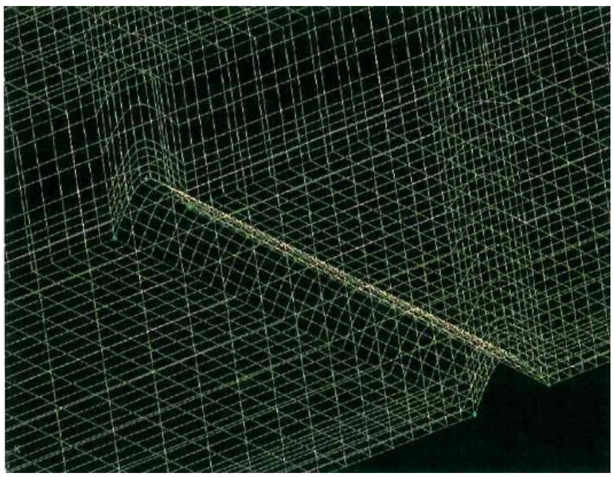

Fig. 5: Mesh size of parabolic ridge

Navier-Stokes equation in Cartesian coordinates in the x, y and z direction can be given by [6],

$$\rho\left(\frac{\partial u}{\partial t}+u\frac{\partial u}{\partial x}+v\frac{\partial u}{\partial y}+w\frac{\partial u}{\partial z}\right)=-\frac{\partial \rho}{\partial x}+\rho g_x+\mu\left(\frac{\partial^2 u}{\partial x^2}+\frac{\partial^2 u}{\partial y^2}+\frac{\partial^2 u}{\partial z^2}\right)$$

$$\rho\left(\frac{\partial v}{\partial t}+u\frac{\partial v}{\partial x}+v\frac{\partial v}{\partial y}+w\frac{\partial v}{\partial z}\right)=-\frac{\partial \rho}{\partial y}+\rho g_y+\mu\left(\frac{\partial^2 v}{\partial x^2}+\frac{\partial^2 v}{\partial y^2}+\frac{\partial^2 v}{\partial z^2}\right)$$

$$\rho\left(\frac{\partial w}{\partial t}+u\frac{\partial w}{\partial x}+v\frac{\partial w}{\partial y}+w\frac{\partial w}{\partial z}\right)=-\frac{\partial \rho}{\partial z}+\rho g_z+\mu\left(\frac{\partial^2 w}{\partial x^2}+\frac{\partial^2 w}{\partial y^2}+\frac{\partial^2 w}{\partial z^2}\right)$$

Large eddy simulation (LES) is a numerical technique used to solve the partial differential equations governing turbulent fluid flow. The turbulent flows are characterized by eddies with a wide range of length and time scales. The largest eddies are typically comparable in size to the characteristic length of the mean flow. The smallest scales are responsible for the dissipation of turbulence kinetic energy. In LES, large eddies are resolved directly, while small eddies are modelled. The rationale behind LES can be summarized as follows:

- Momentum, mass, energy and other passive scalars are transported mostly by large eddies.
- Large eddies are more problem-dependent. They are dictated by the geometries and boundary conditions of the flow involved.
- Small eddies are less dependent on the geometry, tend to be more isotropic and are consequently more universal.
- The chance of finding a universal turbulence model is much higher for small eddies.

The Smagorinsky-Lilly model is a form of LES. This model was first proposed by Smagorinsky. In the Smagorinsky-Lilly model the eddy-viscosity is modeled by $\mu_t = \rho L_s^2 \left|\bar{S}\right|$ where L_s is the mixing length for sub grid scales and $\left|\bar{S}\right| = \sqrt{2\bar{S}_{ij}\bar{S}_{ij}}$. In Fluent L_s is computed using $L_s \min(kd, C_s V^{1/3})$ where k is the von Kármán constant, d is the distance to the closet wall, Cs is the Smagorinsky constant and V is the volume of the computational cell [3].

2.3 Fluent Details

Fluent is a state of the art computer program for modelling fluid flow and heat transfer in complex geometries. Using the six stages mentioned above, the following steps were used for achieving simulation results [3]:

- Import mesh from Gambit
- Check mesh
- Selection of the solver
- Choose the basic equations to be solved
- Specify material properties
- Define operating condition
- Specify boundary conditions
- Define grid interfaces
- Change residual monitors
- Initialize
- Iterate
- Examine results

The boundary conditions for the inlet of the wind tunnel were set for three different tests with Reynolds numbers (Re) of 30000, 60000 and 90000. The respective velocities at the inlet of the simulation of the fluid flows were found using the Reynolds number equation given below,

$$\mathrm{Re} = \frac{\rho V L}{\mu}$$

The fluid density and viscosity of air used were 1.225 kg/m^3 and 1.79 × 10^5 kg/m-sec respectively. The calculated inlet velocities are 1.76 m/s for Re of 30,000; 3.52 m/s for Re of 60,000 and 5.28 m/s for Re of 90,000. The turbulence model used was Large Eddy Simulation with a Smagorinsky constant of 0.1; this was then iterated until the residuals converged.

2.4 Model Validation with Data Available for Circular Ridge

Initially the simulation was done for circular ridge and was verified against data found from literature. If the viscous forces are neglected, the pressure coefficient can be calculated numerically using the inviscid flow theory given below [7, 8],

$$C_P = 1 - 4\sin^2\theta$$

Where, θ is angular coordinate which can only satisfy ideal fluid flow. The fluid inside the boundary layer has less momentum than the fluid outside the boundary layer. The affect is noticeable on the rear of the circular where the pressure does not rise but is approximately constant. This can be seen from the results of the fluid flow over the centre of the circular ridge at three Reynolds numbers, 30000, 60000 and 90000, with the two levels of mesh density, in Figs. 6, 7 and 8 respectively. The graphs of the pressure coefficient are expressed as a function of X/C, where X denotes the distance measured from the lead edge of the surface and C is the width of the corresponding surface. The pressure coefficient results using inviscid theory mentioned above are in good agreement with the simulation results at Reynolds number of 60,000 and thus it is fair to say that the simulation is valid at this Reynolds numbers and/or at 3.52 m/s velocity. It is also to be noted that the results are mesh independent as there is no or negligible difference in the simulated results.

3 Experimental Versus Simulation

3.1 Experimental

The experimental data for parabolic and rectangular ridges was measured by Rasul *et al.* [9] in wind tunnel. The wind tunnel used was an open circuit blower type, driven by a 2.7 hp induction motor at 2900 rpm, with 90x30x20 cm working section. The flow was straightened using flow straightner made of glass tubes (honey comb) in the upstream of the wind tunnel. Two ridges as shown in Fig. 9 (parabolic) and 10 (rectangular), were tested in the wind tunnel [9]. The dimension of rectangular ridge was 30 cm long, 4 cm wide and 2 cm high. The height of parabolic ridge was same as rectangular ridge i.e. 2 cm. A total of 19 probes were introduced on the surface of rectangular ridge: 4 probes on the front surface, 11 probes on the top surface, and 4 on the rear surface. A total of 11 probes were introduced on the surface of parabolic ridge. It is to be pointed out that the equal number of probes was introduced on the surface of the parabolic ridge and top surface of the rectangular ridge. The probe positions were equally spaced and the head of the probes was meshed with the surface of the models (ridges) in order to avoid the disturbance of the flow over the models. Probes were placed diagonally on each surface. Some of the probe positions are shown in Figs. 8 and 9. It was assumed that the boundary layer is uniform along the length of the model at each probe position.

Pressure distribution were monitored over the ridges by using pitot static tube connected to manometer by flexible plastic tube at different Reynolds numbers which was controlled by two wing butterfly valve of the wind tunnel. The Reynolds numbers have been calculated using the height, B, of the ridges as an equivalent geometric dimension. The pressure coefficient, C_p, for bluff bodies can be calculated from measured pressure distribution over the ridges using a formula given below [10, 11],

$$C_p = \frac{\Delta P}{\frac{1}{2}\rho U_0^{\,2}} = \frac{P - P_o}{\frac{1}{2}\rho U_0^{\,2}}$$

where, Δ P is the pressure difference (Pa), P is the pressure on the surface of the ridges (Pa), P_o is the pressure in the undisturbed stream of flow (Pa), ρ is the density of air (kg/m^3), and U_0 is the free stream velocity (m/s).

The C_p was experimentally determined by Rasul *et al* [9] for three different Reynolds number for both of the ridges. These Reynolds numbers were adjusted by keeping butterfly wing approximately full open, half open and three-quarter open. The measured pressure distribution (measured $C_{p)}$ of parabolic ridge as a function of dimensionless parameter X/C is shown in Fig. 11, where X denotes the distance measured from the leading edge of the surface and C is the width of the corresponding surface. It can be seen from Fig. 10 that the pressure distribution, in general, is positive on the front surface and negative on the rear surfaces of the ridge, as expected. At the incidence, the pressure is positive and then starts decreasing. The pressure reaches maximum in the negative direction at X/C of 0.5 i.e. at the middle of surface. But, the pressure never reaches positive and not even the atmospheric at the trailing edge.

Separation starts before the flow reaches the middle of the surface and thus creating vortex or recirculation zone behind the object. The larger is the vortex, the longer it will take the flow to develop fully. The negative pressure distribution at the trailing edge indicates the presence of vortex and its magnitude indicates the relative size of the vortex.

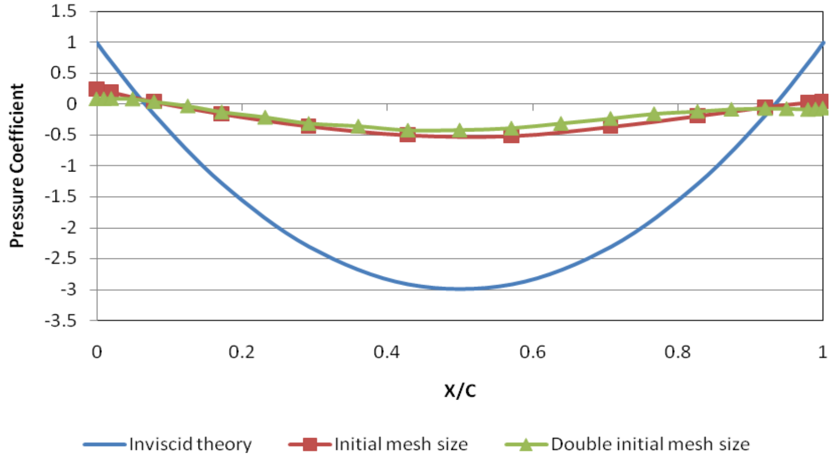

Fig. 6: Pressure coefficient distribution on the circular ridge for a Reynolds number of 30000

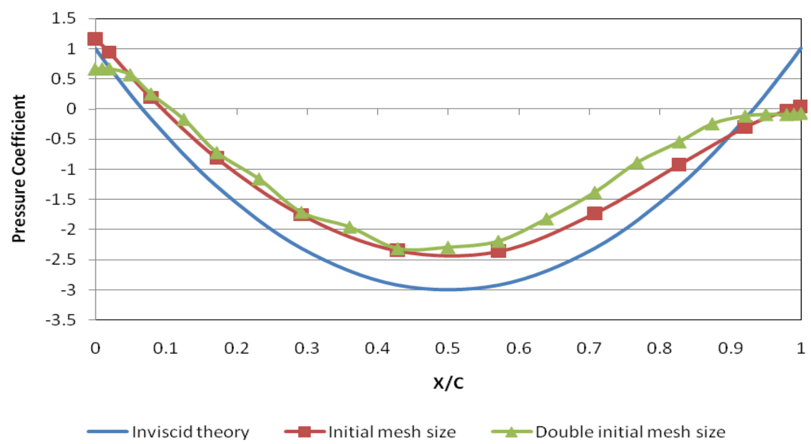

Fig. 7: Pressure Coefficient distribution on the circular ridge for a Reynolds number of 60000

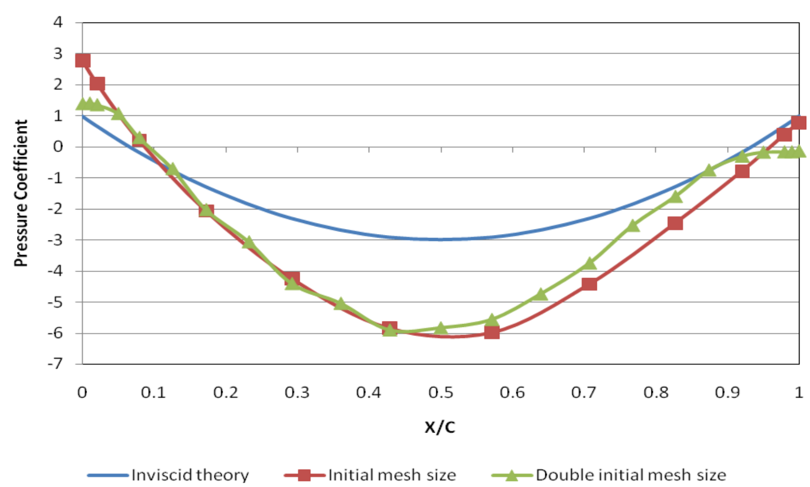

Fig. 8: Pressure Coefficient distribution on the circular ridge for a Reynolds number of 90000

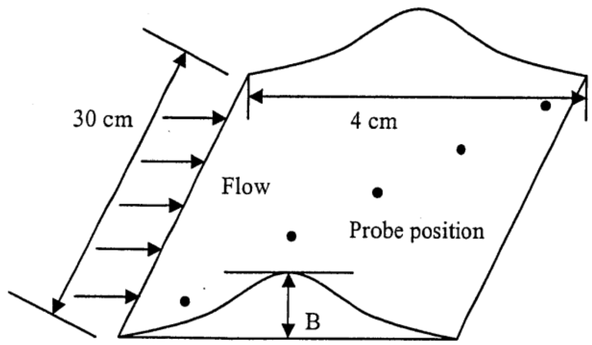

Fig. 9: Schematic views of parabolic ridge

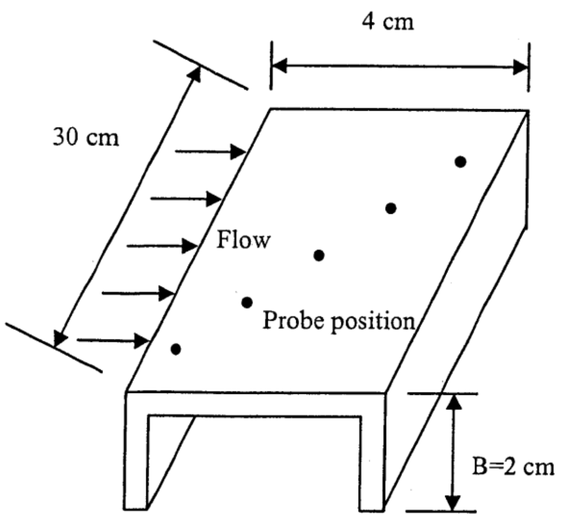

Fig. 10: Schematic views of rectangular ridge

The pressure distribution over a rectangular ridge is shown in Fig. 12. From the figure it is seen that the pressure distribution is positive on the front surface and negative on both top and rear surfaces of the ridge. The pressure distribution over a rectangular ridge is even more complicated but essentially interesting. The leading face displays almost reverse i.e. inverted bucket shape negative pressure distribution. However, the general trend has remained same as the parabolic ridge. The peculiar shape of pressure distribution in the leading surface of the rectangular ridge may be explained as follows. Along the streamline in the plane of symmetry, which leads to the stagnation point, there is a considerable pressure increase in the direction of flow. On the face, no separation occurs because no wall friction is present. But, the flow is diverted up and down once it strikes the surface. The downward flow meets the base plate giving rise to high pressure at the bottom most point. In this case, the separation starts as soon as the top horizontal surface is approached.

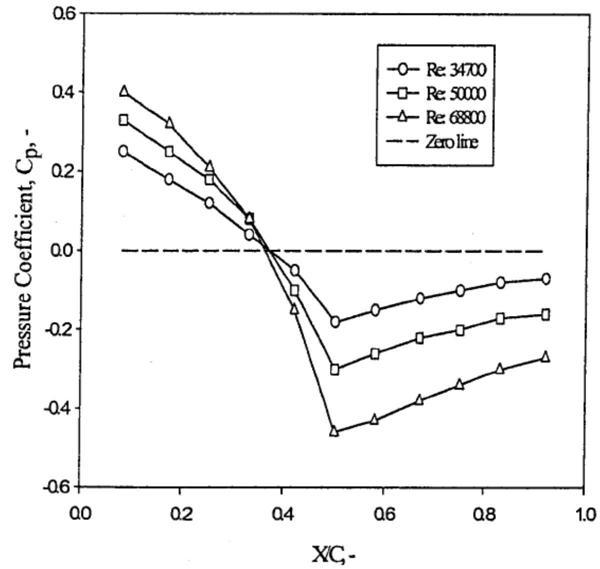

Fig. 11: Pressure distribution on the parabolic ridge

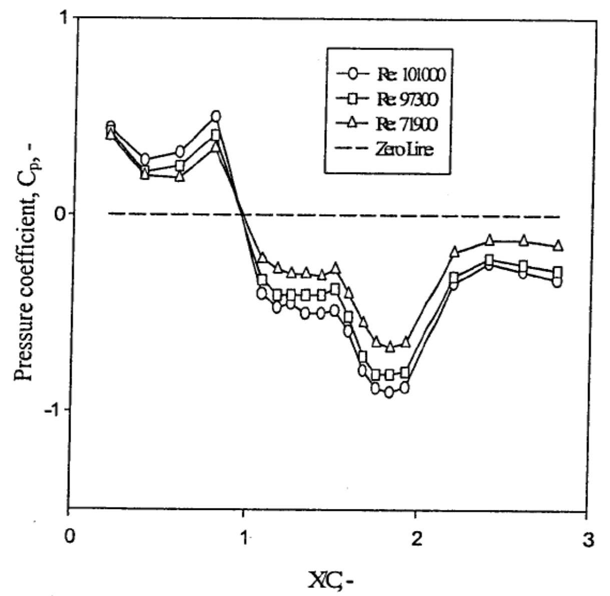

Fig. 12: Pressure distribution on a rectangular ridge

3.2 Simulation

The contour of the pressure coefficient distribution, at three different flow rate of fluid, for parabolic ridge is shown in Figs. 13, 14 and 15. The pressure is positive, in general, on the front of the ridge and negative on the top and rear. It can also be seen that the pressure is more negative in the corners of the ridge than it is in the centre. It is interesting to see that as the fluid flow rate increases, the pressure at the centre of the rear of the ridge increases. The separation point does appear to be affected by this increase. The reason for this is that at higher Reynolds number (14), the pressure drag is less dependent on the Reynolds number.

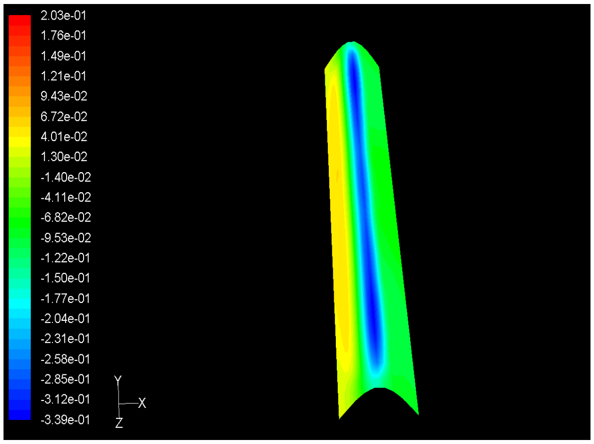

Fig. 13: Pressure coefficient distribution for fluid flow over the parabolic ridge at 1.76 m/s

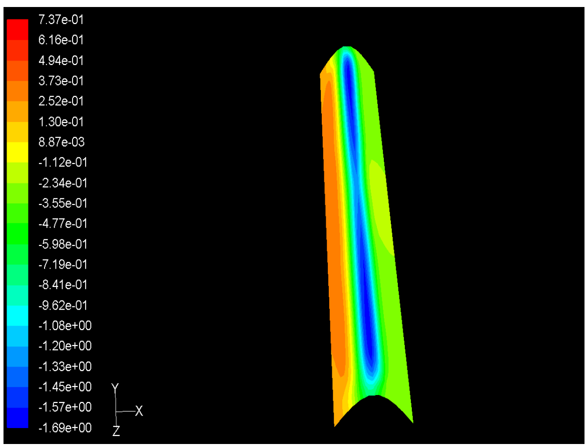

Fig. 14: Pressure coefficient distribution for fluid flow over the parabolic ridge at 3.52 m/s

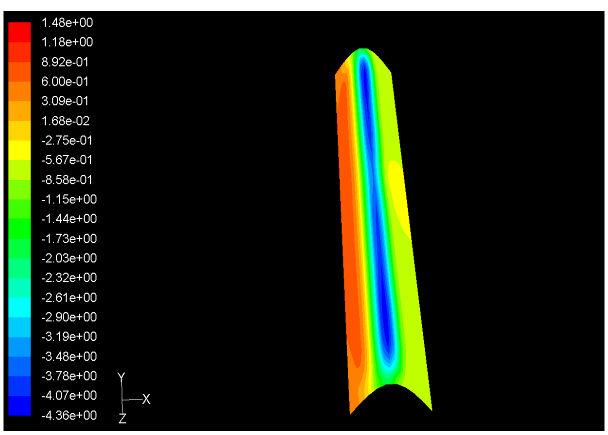

Fig. 15: Pressure coefficient distribution for fluid flow over the parabolic ridge at 5.28 m/s

It is also interesting to see that the width of the pressure drop on the top of the parabolic ridge is thinner near the centre. This is due to the affect of the walls on the velocity magnitude. Therefore the velocity is greater at the centre on the ridge. This effect was further studied by the pressure distribution in the fluid outside of the boundary layer as it flows past the ridge (Fig. 16). This flow was at the Reynolds number of 30,000 and the slices at the increments of 5 millimeters from front edge to the rear edge. These graphs start at X/C of 0 and proceed to 1 with interval of 0.125. It can be seen from Fig. 16 that the pressure distribution in the z-direction is not consistent but symmetrical about the centre. At the rear of the ridge, two pools of pressure drop can be seen. As the fluid flows over the parabolic ridge, the boundary layer protrudes before the fluid particles in the boundary layer loss their momentum. Thus in the pools of pressure drop, the fluid particles are losing more energy than the fluid particles flowing over the centre of the ridge. This could be due to the effects of the wall.

The pressure coefficient distribution over the rectangular ridge is similar to the parabolic ridge; the pressure is positive on the front and negative on the top and rear. This is shown in Figs. 17, 18 and 19. It is seen from Figs. 17, 18 and 19 that the pressure drop which happened on the top of the parabolic ridge, does not happen the same way on the rectangular ridge. This pressure drop only happens on the corner on the front edge and then reduces to an approximately constant pressure for the rest of the top and rear surfaces. This happens because this point is the flow separation location, the fluid inertia becomes more important and at the separation location the fluid's inertia is such that it cannot follow the path after the separation location [11]. As the Reynolds number increases the pressure coefficient drops. This is the same effect which happens to the parabolic shape.

The pressure coefficient distributions for both the parabolic and rectangular ridges at the centre are shown in Figs. 20 and 21 respectively. It can be clearly seen that, though the trend is similar, there are differences in magnitude for both rectangular and parabolic ridges in pressure distributions between experiments and CFD simulations. In comparing the results between CFD simulation and experiment for rectangular ridge, the main difference is that the pressure drop is in a different location. In the experiment pressure drop happens at the rear corner whereas in the CFD simulation the pressure drop happens till just after the top corner. In another word, in the experiment the fluid particles in the boundary layer on the rectangular ridge gain energy at the rear corner of the ridge. In CFD simulation the fluid particles lost most of their energy at this point. This could be due to an unknown element interfering with the wind tunnel experiment. The pressure distribution on the parabolic ridge in the wind tunnel experiment has a steep pressure drop at the top of the ridge, whereas in the CFD simulation this pressure distribution is less steep. The reason for this could be the accurate dimensions for the parabolic ridge in the experiment were not known; only height and width were known. It can be seen from Fig. 9 that the top of the ridge is steeper; this may have accounted differently in CFD simulation. Although, the text book information fairly supports the pressure distribution of the CFD simulation, further study is recommended in order to find out the reason for variation between experimental results and CFD simulation results.

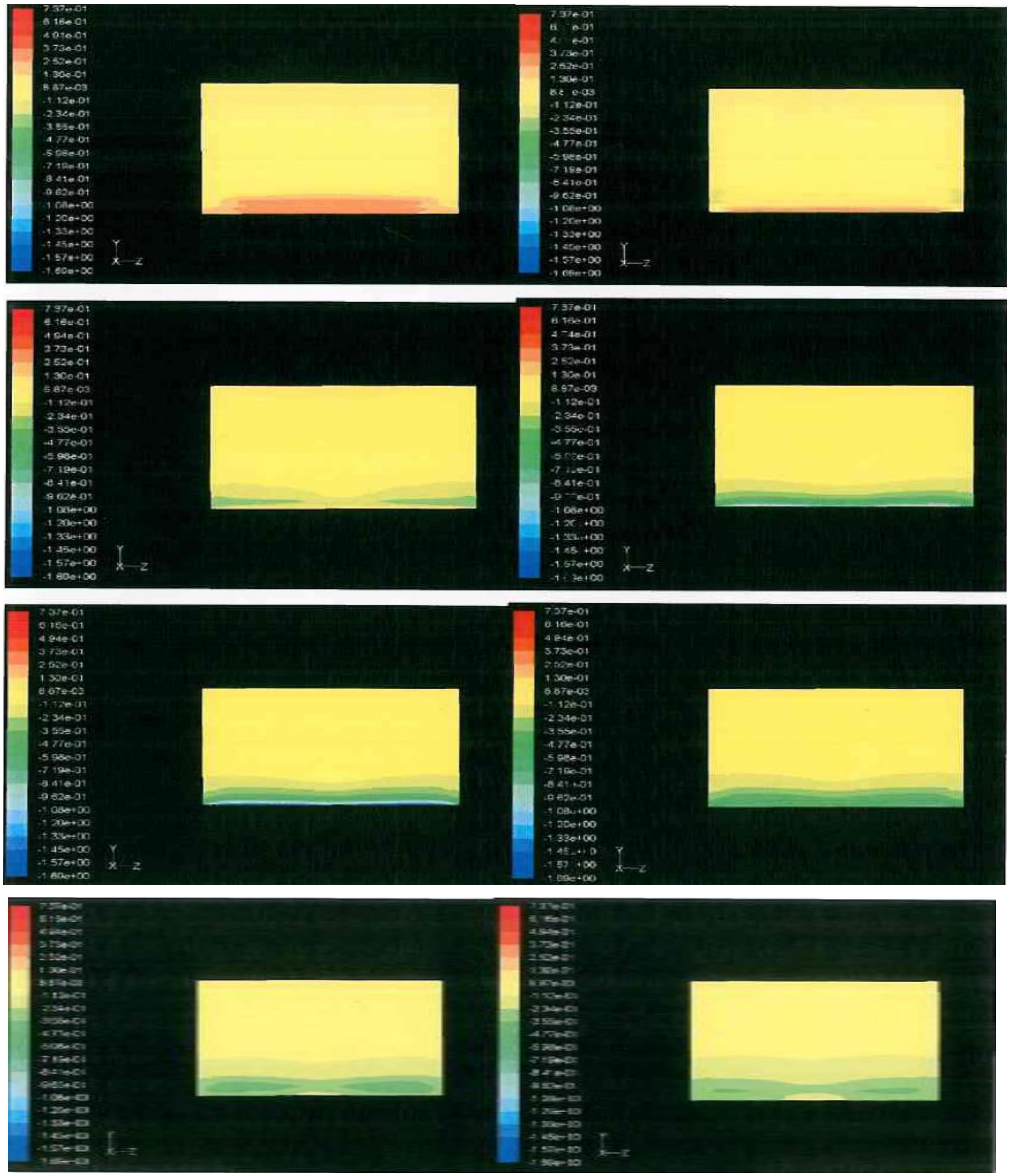

Figure 16: Pressure distribution contours for parabolic ridge at different X/C intervals

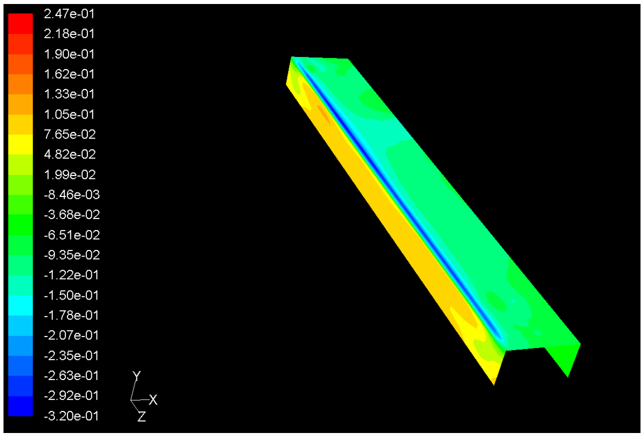

Fig. 17: Pressure coefficient distribution for fluid flow over the rectangular ridge at 1.76 m/s

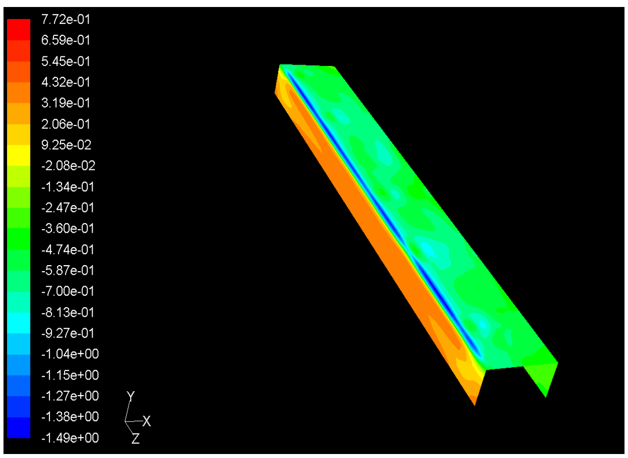

Fig. 18: Pressure coefficient distribution for fluid flow over the rectangular ridge at 3.52 m/s

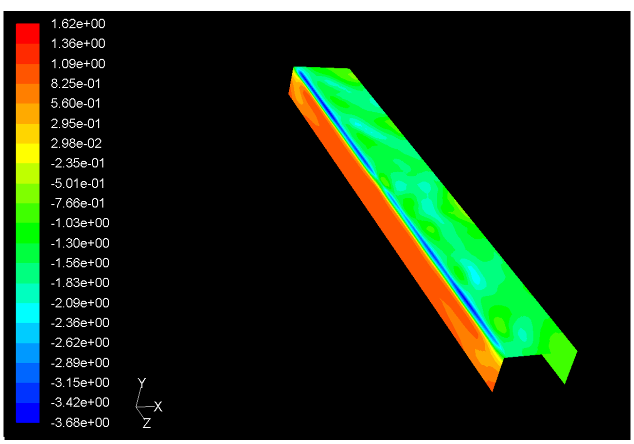

Fig. 19: Pressure coefficient distribution for fluid flow over the rectangular ridge at 5.28 m/s

4 Conclusions

This study has shown that a bluff body submerged in fluid experiences a pressure distribution with respect to the bodies shape. The simulation of both the parabolic and rectangular ridges in Fluent has shown that there are differences in the results between CFD simulation and wind tunnel experiments. One of the reasons for these differences could be due to the fact that the inlet distance was increased by 3m for the CFD simulation and therefore the flow would be more developed. The wall roughness was also not taken into consideration for the CFD simulation, which could have an influence on the boundary layer flow.

Nomenclature

P	Pressure (Pa)
$\vec{V}$	Fluid flow velocity vector
{u,v,q}	Fluid flow velocity components
{x,y,z}	Cartesian coordinates
τ	Time
ρ	Density (kg/m^3)
g	Gravitational force (m/s2)
Cp	Pressure coefficient (-)
ΔP	Pressure difference (Pa)
P_o	Pressure in undisturbed stream of flow (Pa)
U_o	Free stream velocity (m/s)

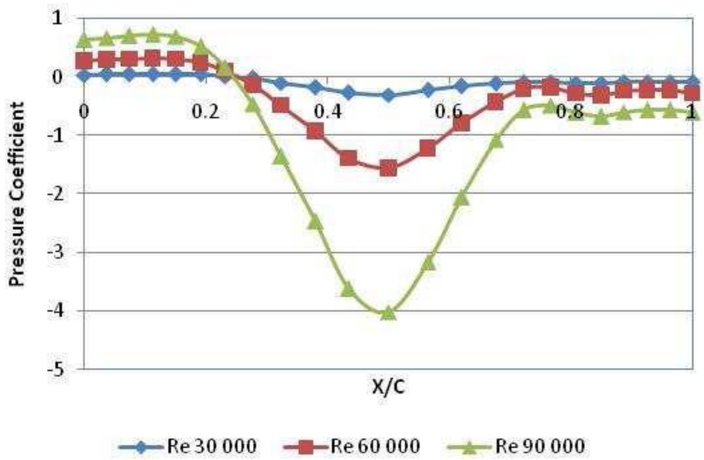

Fig. 20: Simulated pressure co-efficient distribution for rectangular ridge

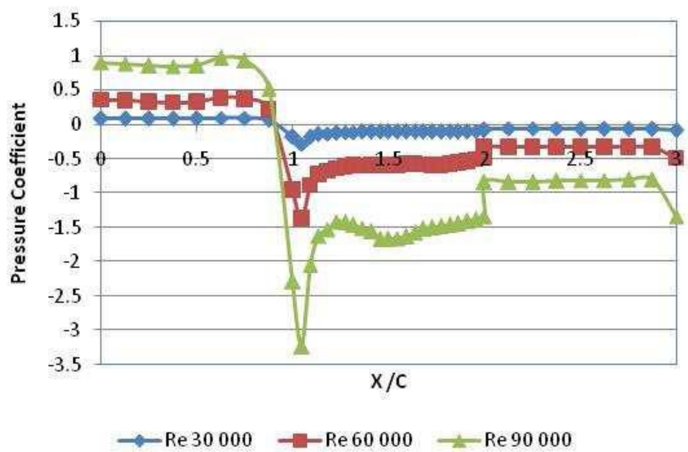

Fig. 21: Simulated pressure co-efficient distribution for parabolic ridge

References

[1] Baker, A.J. and Gordon, E.B., 1997, Computational fluid dynamics - a two-edged sword, *ASHRAE Journal, 39(8), 51-58*.

[2] Chen, Q., 1997, Computational fluid dynamics for HVAC - successes and failures, *ASHRAE Transactions, 103(1), 178-187*.

[3] Fluent, 2005, “Fluent 6.2 user’s Guide”, Reaction Design Inc., Labanon USA.

[4] Versteeg, H and Malalasekera, W., 2007, An introduction to computational fluid dynamics: The finite volume method, *Pearson Education Limited*, Essex.

[5] Cengel, Y. and Cimbala, J.M., 2006, *Fluid Mechanics – Fundamentals and applications*, McGraw-Hill, USA.

[6] Gerhart, P.M. and Gross R.J., 1985, *Fundamentals of Fluid Mechanics*, Addison-Wesley Publishing Company Inc., USA

[7] Munson, B.R., Young, .F.Y. and Okiishi, T.H, 2002, *Fundamentals of Fluid Mechanics*, John Wiley & Sons, Inc. USA

[8] Hoener, F., 1965, *Fluid Dynamics Drag*, 2nd Edition, NJ, Part 3.

[9] Rasul, M.G., Khan, M.M.K. and Das, D.K, 2003, Comparison of pressure distribution over ridges in a wind tunnel, *2nd International Conference on Heat Transfer, Fluid Mechanics and Thermodynamics*, *Paper Number: RM1*, 23-26 June, Victoria Falls, Zambia.

[10] Street, R.L., Walters, G.Z. and Vennard, J.K. 1996, *Elementary Fluid mechanics*, 7th edition, John Wiley & Sons, New York.

[11] Abbott, I.H. and Von Docnhoff, A.E., 1959, *Theory of wings sections including a summary of aerofoil data, pp. 31-45*, Dover Publications Inc. New York.